AGU PUBLICATIONS

Paleoceanography

RESEARCH ARTICLE
10.1002/2013PA002578

Key Points:
- Deep water renewal within the SCS since the last glacial period
- Evidence for the deglacial northern sourced North Pacific deep water
- New insights into deep circulation and carbon cycle evolution in the Pacific

Correspondence to:
Z. Jian,
jian@tongji.edu.cn

Citation:
Wan, S., and Z. Jian (2014), Deep water exchanges between the South China Sea and the Pacific since the last glacial period, *Paleoceanography*, *29*, 1162–1178, doi:10.1002/2013PA002578.

Received 6 NOV 2013
Accepted 13 NOV 2014
Accepted article online 19 NOV 2014
Published online 9 DEC 2014

Deep water exchanges between the South China Sea and the Pacific since the last glacial period

Sui Wan[1] and Zhimin Jian[1]

[1]State Key Laboratory of Marine Geology, Tongji University, Shanghai, China

Abstract Deep ocean circulation is widely considered as one of the important factors for increasing CO_2 concentration and decreasing radiocarbon activity ($\Delta^{14}C$) of the atmosphere during the last deglaciation. The AMS ^{14}C ages of benthic and planktonic foraminifers from 18 samples of Core MD05-2904 (water depth of 2066 m) in the northern South China Sea (SCS) and 15 samples of Core MD05-2896 (water depth of 1657 m) in the southern SCS were analyzed in this study for reconstructing the intrabasin deep oceanic processes and hence exploring the deep water exchanges between the SCS and the Pacific since the last glacial period. The results show that during the Holocene the average apparent ventilation age of deep water was younger in the southern SCS (~1350 years) than in the northern SCS (~1850 years) due to relatively strong vertical mixing and advection, consistent with modern observations. However, during the last glacial period and deglaciation the deep water was older in the southern SCS (~2050 years and ~1800 to 1200 years, respectively) than in the northern SCS (~1600 years and ~670 years, respectively), indicating reduced deep mixing and advection. Moreover, the northern SCS deep water was significantly younger during the last deglaciation than during the Holocene and the last glacial period, implying the existence of northern sourced newly formed and relatively young North Pacific deep water. Our records do not support the intrusion of anomalously ^{14}C-depleted deep water to the middepth of the low-latitude western Pacific and the SCS during the "Mystery Interval" (17.5–14.5 kyr B.P.).

1. Introduction

The major carbon reservoir in the deep ocean is believed to play a primary and significant role in regulating atmospheric CO_2 concentration and $\Delta^{14}C$ activity [*Broecker*, 1982; *Sigman and Boyle*, 2000]. For example, the remarkable global climatic and oceanic shifts during Heinrich Stadial 1 (HS1, the so-called "Mystery Interval"; 17.5–14.5 kyr B.P.) of the last deglaciation, when atmospheric radiocarbon activity ($\Delta^{14}C$) experienced a ~190‰ drop rapidly with a remarkable atmospheric CO_2 rise of ~50 ppm [*Broecker and Barker*, 2007; *Monnin et al.*, 2001], was widely attributed to the reorganization of deep ocean circulation which allowed glacial ^{14}C-depleted carbon somewhere within the isolated deep ocean to mix back into upper ocean and atmosphere in the deglaciation [*Skinner et al.*, 2010]. In recent studies, the ^{14}C-depleted deep water originating likely in the Southern Ocean are found to have been incorporated into intermediate and even thermocline waters and spread northward into the low-latitude eastern Pacific [*Marchitto et al.*, 2007; *Stott et al.*, 2009], northern Arabian Sea [*Bryan et al.*, 2010] and high-latitude Atlantic Ocean [*Thornalley et al.*, 2011] during HS1. However, the influence of the aged and ^{14}C-depleted deep water was rather limited in spatial extent. Records from the western Pacific have generally exhibited deep ocean ^{14}C depletion similar to or only slightly greater than corresponding modern level [*Broecker et al.*, 2004a, 2004b, 2007, 2008; *Galbraith et al.*, 2007].

Furthermore, during HS1 the Pacific deep water could be locally formed in the North Pacific rather than coming from the North Atlantic via the Southern Ocean. The newly formed North Pacific deep water could even extend to a depth of ~3600 m according to a compilation of radiocarbon records and modeling simulations [*Okazaki et al.*, 2010; *Sarnthein*, 2011; *Rae et al.*, 2014]. The simulated deep water pathway spread southward along the western margin of the North Pacific, forming a simple western boundary deep current system [*Okazaki et al.*, 2010], and probably entering the South China Sea (SCS) through the Luzon Strait and becoming one of the main sources for the SCS deep water [*Lüdmann et al.*, 2005; *Sarnthein et al.*, 2013a, 2013b]. A switch of deep water formation between the North Atlantic and the North Pacific would have a key impact on regulating oceanic heat transport and deep ocean carbon exchange during the last deglaciation. This has become one of the vigorous debated issues for paleoceanographic and paleoclimatological study in recent years.

Until now, our knowledge of deep water structure change and paleoventilation history in the Pacific, particularly in the low-latitude western Pacific, is very limited mainly due to poor preservation and low sedimentation of carbonate sediments. The SCS as the biggest low-latitude marginal sea of the western Pacific has sedimentation rates higher by an order of magnitude than the Pacific, and its extensive carbonate sediments can provide favorable materials (containing enough benthic foraminiferal shells for the accelerator mass spectrometry AMS ^{14}C dating) for reconstructing the history of deep water renewal. Particularly, the Luzon Strait with a sill depth of about 2600 m serves as the only gateway of deep water exchange between the SCS and the Pacific, offering a unique opportunity to monitor the western Pacific deep water variations [*Chao et al*., 1996; *Jian and Wang*, 1997].

Previous studies mainly based on the analyses of deep-sea benthic foraminiferal assemblages and stable isotopes have provided some information on deep water changes in the western Pacific and the SCS during late Quaternary glacial-interglacial cycles [*Jian and Wang*, 1997; *Jian et al*., 1999; *Oppo and Fairbanks*, 1987; *Wei et al*., 2006]. Among them, *Broecker et al*. [1988, 1990] and *Andree et al*. [1986] first analyzed the planktic and benthic foraminiferal radiocarbon records of Cores V35-5, V35-6, and SO50-37KL in the SCS, and revealed preliminarily that the ages of glacial deep water in the SCS were close to or a little greater than those in the Holocene, but the deglacial and glacial records of deep water renewal are still considerably lacking because of scarce radiocarbon data and variable sedimentary material quality [*Broecker et al*., 2006]. In this study, we present a detailed account of deep water variations of apparent ventilation age in the SCS since the last glacial period, mainly based on comprehensive analyses of radiocarbon records from coexisting planktic and benthic foraminifera in the northern and southern SCS, aiming to discuss the deep water exchange between the SCS and the Pacific with the focus on potential influence on the basin's deep water by the external (Pacific deep water changes) and internal renewal (vertical mixing and advection) processes in the past.

2. Oceanographic Settings

Modern oceanic investigations have demonstrated that the low-latitude western Pacific deep ocean (~1500–2500 m) [*Wyrtki*, 1961; *Emery*, 2001] is filled dominantly by the southern Upper Circumpolar Deep Water (UCDW) from the Southern Ocean but not the modified North Pacific Deep Water (NPDW) [*Kawabe and Fujio*, 2010] (Figure 1a). The western Pacific deep water crosses the only deep channel Luzon Strait, sinks, spreads out, and fills the SCS deep basin [*Qu et al*., 2006]. The SCS deep water is believed to upwell into the intermediate water between 350 and 1350 m, which is then exported out of the SCS again into the western Pacific through the Luzon Strait [*Su*, 2004]. The vertical transect of the net flow volume through the Luzon Strait displays a sandwiched structure [*Tian et al*., 2006]: waters enter the SCS in the deep layer (>1500 m) and flow out of the SCS into the Pacific in the intermediate layer (500–1500 m), which are regarded as the deep and intermediate waters in the SCS, respectively (Figure 1b).

According to the historical hydrographic data from the western Pacific and the SCS, the modern inflow deep water is primarily a mixture of Circumpolar Deep Water (CDW) and Pacific Subarctic Intermediate Water, both as defined by *Emery* [2001] [*Chang et al*., 2010]. The SCS deep water counterclockwise flows within the basin and is estimated to have a fast flushing time of 40–50 years [*Chen et al*., 2001] or 30–71 years [*Chang et al*., 2010], or even less than 30 years [*Qu et al*., 2006]. Therefore, the modern SCS deep water has efficient and rapid renewal associated with internal processes involving vertical mixing, deep upwelling, and advection. An oxygen minimum zone exists between approximately 500 and 1500 m, with lowest oxygen concentration being below ~1.5 mL/L in the south. The physical properties of the intermediate water mass are very similar to those of western North Pacific intermediate water with ranges of between 11°C and 3°C in temperature and from 34.50‰ to 34.60‰ in salinity. The deep water is derived the western Pacific Deep Water (PDW) and has fairly uniform properties with minor changes in temperature and salinity. The deep water oxygen concentration increases slightly with depth to values of approximately 2.0 mL/L, revealing the relatively rapid renewal of the SCS [*Wyrtki*, 1961] (Figure 1).

Shell δ^{13}C of benthic foraminiferal species *Cibicidoides wuellerstorfi* is considered the most reliable indicator of seawater δ^{13}C [*Duplessy et al*., 1984; *Tachikawa and Elderfield*, 2002]. The shell δ^{13}C data in *C. wuellerstorfi* from the surface sediments also reveal the hydrographic structure and internal processes in the modern SCS [*Cheng et al*., 2005] (Figure 1b). The modern δ^{13}C distribution seems to be dominated by organic matter

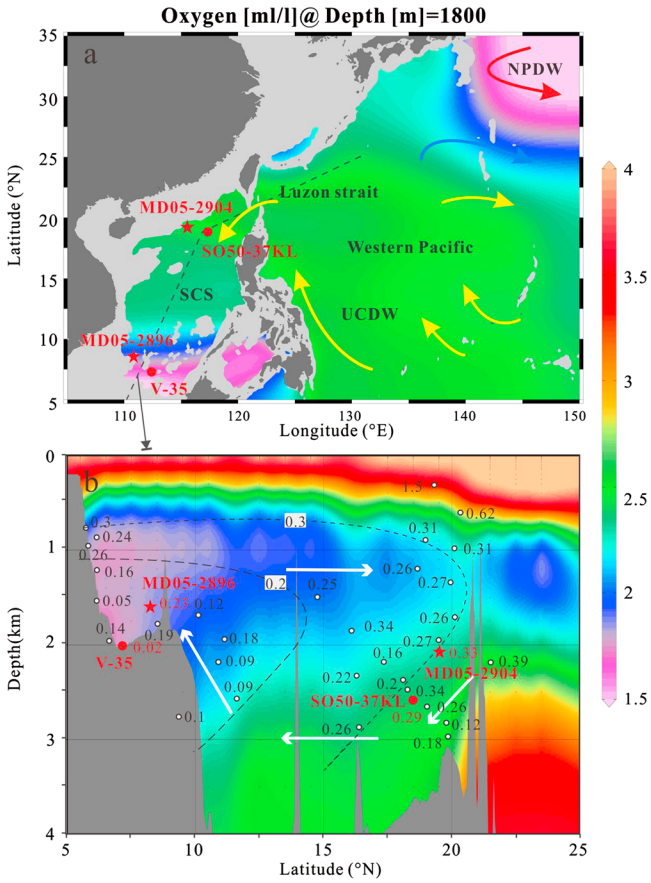

Figure 1. Location of cores and regional oceanographic settings. The colors of oceanic background show oxygen concentration at depth of 1800 m based on World Ocean Atlas 2009 [*Garcia et al.*, 2010], redrawn by Ocean Data View 4 (Schlitzer R, available at http://odv.awi.de). (a) Arrows indicate the deep circulaton in the low-latitude western Pacific after *Kawabe and Fujio* [2010]. Red, orange, and blue arrows represent North Pacific Deep Water (NPDW), Upper Circumpolar Deep Water (UCDW), and the transition between NPDW and UCDW, respectively. Red stars and dots denote location of the SCS cores in this and previous studies, respectively. (b) Meridional bathymetric profile (along the dashed line in Figure 1a) of oxygen content in the SCS, indicating the distribution of the intermediate and deep water masses. Circles indicate the δ^{13}C of *C.wuellerstorfi* from the surface sediments in the SCS [*Cheng et al.*, 2005]. The numbers nearby are the δ^{13}C values in the involved locations. Dashed lines show the estimated δ^{13}C contours. White arrows mark the simplified deep circulation.

remineralization, generally consistent with the oxygen content profile. There is a north-south δ^{13}C gradient of ~0.2‰ along the deep inflow path while an opposite slight gradient in the intermediate outflow direction.

3. Material and Methods

3.1. Sediment Samples

The samples used in this study were collected from two sediment cores of the northern and southern SCS: Calypso gravity Core MD05-2904 (19°27.32′N, 116°15.15′E; water depth of 2066 m; core length 44.98 m) and CASQ Core MD05-2896 (8°49.5′N, 111°26.47′E; water depth of 1657 m; core length 11.03 m) taken during R/V *Marion Dufresne* 147/IMAGES XII-MARCO POLO in 2005 [*Laj et al.*, 2005] (Figure 1). Sediments in these cores are composed mainly of dark olive-grey homogeneous silty clay. No slumping structures or mass transport have been found in the sediment core.

The two studied cores have been analyzed for reconstructing past changes of the East Asian monsoon at the orbital and millennial time scales based on planktic foraminiferal δ^{18}O and Mg/Ca records [*Ge et al.*, 2010; *Steinke et al.*, 2011; *Tian et al.*, 2010], providing well-established stratigraphic framework for this study. Particularly, the two cores bathed in the SCS deep water, contain enough benthic foraminiferal shells for the AMS ^{14}C dating in most of the samples, offering an unprecedented opportunity to reconstruct the SCS deep water variations since the last glacial period.

3.2. Radiocarbon Dating

Well-preserved foraminiferal shells were picked from the >154 μm fraction of previously washed sediment samples of Cores MD05-2904 and MD05-2896 for the AMS ^{14}C dating. Planktic foraminiferal species *Globigerinoides ruber* (800–1000 shells, no size limits) and mixed species of benthic foraminifera (weight >5 mg) were used in this study. The benthic foraminifera were mostly epifaunal and shallow-to-intermediate infaunal species, including *Cibicidoides* spp., *Oridosalis umbonatus*, *Epistominella exigua*, *Uvigerina* spp., *Osangularia culter*, *Globocassidulina subglobosa*, *Hoeglundina elegans*, *Pullenia* spp., *Bulimina* spp., and *Melonis* spp. Deep infaunal such as *Globobulimina* was not selected. When the benthic foraminiferal numbers were occasionally insufficient, we picked additional shells from adjoining sediment samples to combine a single sample for radiocarbon analysis. To take into account the weighting of benthic shells from each subsample, the planktonics were combined in the same proportions to yield single samples for most of the mixed foraminiferal samples. When a pair of planktonic and benthic samples had different intervals, it should be

Table 1. Plantonic Foraminferal Radiocarbon Dates of Cores: MD05-2904, MD05-2896, SO50-37KL [*Broecker et al.*, 1990; *Sarnthein et al.*, 2007], and V35-6 (Selected Data Points Without Reworked Foraminiferal Shells) [*Andree et al.*, 1986; *Broecker et al.*, 2006][a]

AMS Laboratory Number	Core Depth (cm)	Composite Depth (cm)	Foraminiferal Species	Planktic Weight (mg)	Original ^{14}C Age (year)	$\pm1\sigma$ (year)	Calendar Age (year B.P.)	-1σ (year)	$+1\sigma$ (year)	Remarks
Core MD05-2904 (19°27.32′N, 116°15.15′E; Water Depth of 2066 m)										
Beta-312105	5.5	3–8	*G. ruber*	8.09	1,260	30	654	280	278	
GZ2555	16.5	15–18	*G. ruber*		1,821	30	1,183	307	316	*Ge et al.* [2010]
Beta-312107	61.5	59–64	*G. ruber*	6.93	3,390	40	3,009	338	391	
Beta-312109	107.5	105–110	*G. ruber*	7.34	4,630	40	4,587	430	383	
Beta-312111	257.5	255–260	*G. ruber*	8.95	8,450	40	8,808	394	332	
GZ2556	300.5	299–302	*G. ruber*		9,756	60	10,414	384	402	*Ge et al.* [2010]
Beta-312113	339.5	337–342	*G. ruber*	13.39	10,090	50	10,838	370	359	
Beta-312115	399.5	397–402	*G. ruber*	14.87	12,370	50	13,648	351	289	
GZ2557	480.5	479–482	*G. ruber*		13,433	43	15,367	582	755	*Ge et al.* [2010]
Beta-312118	539.5	537–542	*G. ruber*	11.06	13,620	60	15,721	561	658	
GZ2558	647.5	646–649	*G. ruber*		15,211	80	17,771	390	286	*Ge et al.* [2010]
Beta-330566	704.5	702–707	*G. ruber*	12.54	17,540	80	20,123	340	310	?
GZ2559	763.5	762–765	*G. ruber*		16,675	80	19,205	329	247	?; *Ge et al.* [2010]
Beta-330568	777.5	776–779	*G. ruber*	8.98	18,620	70	21,519	333,396	548	
Beta-330570	819.5	818–821	*G. ruber*	7.06	19,440	80	22,489	396	492	
Beta-321233	844.5	843–846	*G. ruber*	11.29	20,090	80	23,225	316	443	
Beta-321235	910.5	909–912	*G. ruber*	12.54	20,610	80	23,898	365	391	
GZ2660	987.5	986–989	*G. ruber*		21,708	101	25,232	418	492	*Ge et al.* [2010]
GZ2661	1,083.5	1082–1085	*G. ruber*		22,558	132	26,389	515	475	*Ge et al.* [2010]
Beta-312122	1,127.5	1126–1129	*G. ruber*	9.34	26,370	130	30,573	253	324	Abnormal
Beta-312124	1,219.5	1218–1221	*G. ruber*	9.73	26,430	130	30,619	252	302	
Core MD05-2896 (8°49.5′N, 111°26.47′E; Water Depth of 1657 m)										
Beta-321237	19.5	17–22	*G. ruber*	10.74	3,160	30	2,724	390	356	
KIA 32651	49.5	49–50	*G. ruber*		6,315	50	6,566	329	351	*Tian et al.* [2010]
KIA 32650	81.5	81–82	*G. ruber*	7.79	9,465	60	10,040	384	369	*Tian et al.* [2010]
Beta-321241	91.5	89–94	*G. ruber*		11,680	40	12,954	285	280	
KIA 32649	103.5	103–104	*G. ruber*		13,110	90	14,695	637	442	*Tian et al.* [2010]
KIA 32648	129.5	129–130	*G. ruber*	9.04	14,700	100	17,235	357	325	*Tian et al.* [2010]
Beta-321245	141.5	139–144	*G. ruber*	10.38	15,320	70	17,905	355	236	
Beta-330572	169.5	167–172	*G. ruber*	8.07	17,760	70	20,430	428	559	
Beta-330574	181.5	179–184	*G. ruber*	10.42	18,300	70	21,046	225	392	
Beta-330576	193.5	191–196	*G. ruber*	8.56	18,440	70	21,244	419	339	
Beta-321255	209.5	207–212	*G. ruber*		21,180	90	24,563	353	415	
Beta-321253	241.5	239–244	*G. ruber*	11.00	23,120	110	27,188	424	539	
Beta-321251	268.5	266–271	*G. ruber*	9.82	24,150	130	28,338	387	306	
Beta-321249	282.5	280–285	*G. ruber*	8.53	19,370	70	22,387	408	327	Abnormal
Beta-321247	302.5	300–305	*G. ruber*	7.55	24,990	110	29,185	389	348	
Beta-321257	330.5	328–333	*G. ruber*	11.74	30,690	170	34,730	206	292	
Core SO50-37KL (18.76°N, 115.76°E; Water Depth of 2695 m)										
	10.5	8–13	*G. sacculifer*		2,040	70	1,419	352	320	Reanalyzed
	42.5	40–45	*G. sacculifer*		5,960	80	6,166	335	353	
	157.5	155–160	*G. sacculifer*		12,730	140	14,158	537	485	
	162.5	160–165	*G. sacculifer*		15,140	150	17,689	510	344	
	177.5	175–180	*G. sacculifer*		15,910	110	18,497	443	329	
	187.5	185–190	*G. sacculifer*		16,000	120	18,604	535	298	
	197.5	195–200	*G. sacculifer*		17,460	160	20,041	471	310	
	207.5	205–210	*G. sacculifer*		17,660	180	20,296	696	595	
Core V35-6 (7.2°N, 112.2°E; Water Depth of 2030 m)										
	10.5	8–13	*G. sacculifer*		4,860	90	4,887	390	421	Reanalyzed
	41	37–45	*G. sacculifer*		7,890	110	8,173	353	320	
	60.5	57–64	*G. sacculifer*		9,550	120	10,147	421	383	
	70	68–72	*G. sacculifer*		10,130	120	10,891	456	354	
	90.5	89–92	*G. sacculifer*		11,590	140	12,863	280	374	
	100	98–102	*G. sacculifer*		12,540	160	13,879	555	353	

[a]Question marks denote possible anomalous points due to the reversed ages.

Table 2. Benthic Foraminiferal Radiocarbon Dates, Estimates of B-P Age, Deep Water $\Delta^{14}C$ of Cores: MD05-2904, MD05-2896, SO50-37KL [*Broecker et al.*, 1990; *Sarnthein et al.*, 2007], and V35-6 (Selected Data Points Without Reworked Foraminiferal Shells) [*Andree et al.*, 1986; *Broecker et al.*, 2006][a]

AMS Laboratory Number	Core Depth (cm)	Composite Depth (cm)	Benthic Weight (mg)	Benthic ^{14}C Age (yr)	±1σ (year)	Planktic ^{14}C Age (year)	±1σ (year)	B-P Age (year)	±1σ (year)	Deep $\Delta^{14}C$ (‰)	−1σ (‰)	+1σ (‰)	Remark
Core MD05-2904 (19°27.32′N, 116°15.15′E; Water Depth of 2066 m)													
Beta-312104	5.5	3–8	5.65	3,120	30	1,260	30	1860	42	−265.9	25	25	
Beta-312106	61.5	59–64	6.10	4,750	40	3,390	40	1360	57	−203.4	33	38	
Beta-312108	107.5	105–110	7.11	6,260	40	4,630	40	1630	57	−201.0	42	37	
Beta-312110	257.5	255–260	10.30	10,470	50	8,450	40	2020	64	−212.0	38	32	
Beta-312112	339.5	335–344	7.39	10,750	50	10,090	50	660	71	−25.7	48	42	
Beta-312114	399.5	395–404	7.81	12,750	60	12,370	50	380	78	68.6	47	41	
Beta-312116	480.5	479–482	7.05	14,140	80	13,433	43	707	91	87.2	66	75	
Beta-312117	539.5	535–544	7.64	14,260	60	13,620	60	640	85	110.9	57	70	
Beta-321230	647.5	646–649	13.70	15,350	60	15,211	80	139	100	268.8	57	63	
Beta-330565	704.5	701–708	6.79	1,7900	90	17,540	80	360	120	276.0	62	60	?
Beta-312119	763.5	762–765	10.17	18,750	80	16,675	80	2075	113	12.6	50	42	?
Beta-330567	777.5	775–780	7.23	20,260	80	18,620	70	1640	106	121.7	48	60	
Beta-330569	819.5	817–822	7.77	20,770	120	19,440	80	1330	144	179.5	53	51	
Beta-321232	844.5	842–847	10.66	19,670	70	20,090	80	−420	106				Deleted
Beta-321234	910.5	908–913	13.40	20,580	90	20,610	80	−30	120				Deleted
Beta-312120	987.5	986–989	8.27	22,150	100	21,708	101	442	142	368.4	53	68	
Beta-312121	1,127.5	1125–1130	8.43	25,270	120	26,370	130	−1100	177				Deleted
Beta-312123	1,219.5	1217–1222	9.96	26,730	130	26,430	130	300	184	358.0	71	73	
Core MD05-2896 (8°49.5′N, 111°26.47′E; Water Depth of 1657 m)													
Beta-321236	19.5	17–22	14.62	4,370	30	3,160	30	1,210	42	−193.2	38	35	
Beta-321238	49.5	47–52	13.10	7,650	40	6,315	50	1,335	64	−146.2	34	36	
Beta-321240	91.5	79–84	9.01	13,390	60	11,680	40	1,710	72	−93.8	32	31	
Beta-321242	103.5	101–106	5.98	14,620	50	13,110	90	1,510	103	−39.6	64	54	
Beta-321243	129.5	127–132	6.33	16,610	60	14,700	100	1,910	117	0.9	54	55	
Beta-321244	141.5	139–144	13.19	17,130	60	15,320	70	1,810	92	33.3	44	49	
Beta-330571	169.5	167–172	6.19	19,470	80	17,760	70	1,710	106	85.5	57	51	
Beta-330573	181.5	179–184	9.04	20,320	80	18,300	70	2,020	106	60.6	52	54	
Beta-330575	193.5	191–196	10.42	20,920	80	18,440	70	2,480	106	5.4	54	48	
Beta-321254	209.5	207–212	7.96	23,320	90	21,180	90	2,140	127	99.6	54	55	
Beta-321252	241.5	239–244	13.35	25,170	110	23,120	110	2,050	156	114.5	48	55	Deleted
Beta-321250	268.5	266–271	6.36	26,250	120	24,150	130	2,100	177	87.7	39	35	
Beta-321248	282.5	280–285	7.54	15,290	60	19,370	70	−4,080	148				
Beta-321246	302.5	300–305	6.97	27,650	130	24,990	110	2,660	170	−4.9	44	40	
Beta-321256	330.5	328–333	8.75	32,420	240	30,690	170	1,730	294	100.8	50	50	
Core SO50-37KL (18.76°N, 115.76°E; Water Depth of 2695 m)													
	10.5	8–13		3,970	80	2,040	70	1,930	106	−275.6	32	29	Reanalyzed
	42.5	40–45		8,270	100	5,960	80	2,310	128	−247.0	32	33	
	157.5	155–160		13,710	120	12,730	140	980	184	8.7	66	63	
	162.5	160–165		17,100	220	15,140	150	1,960	266	9.0	59	58	
	177.5	175–180		17,430	140	15,910	110	1,520	178	76.4	49	48	
	187.5	185–190		17,590	140	16,000	120	1,590	184	68.0	51	48	
	197.5	195–200		18,940	160	17,460	160	1,480	226	108.3	60	61	
	207.5	205–210		19,445	190	17,660	180	1,785	262	72.7	66	59	
Core V35-6 (7.2°N, 112.2°E; Water Depth of 2030 m)													
	10.5	8–13		6,420	100	4,860	90	1,560	135	−187.8	40	42	Reanalyzed
	41	37–45		9,210	130	7,890	110	1,320	170	−146.2	39	35	
	60.5	57–64		10,810	150	9,550	120	1,260	192	−110.6	49	46	
	70	68–72		11,290	150	10,130	120	1,160	192	−82.7	56	44	
	90.5	89–92		12,950	160	11,590	140	1,360	213	−53.4	38	46	
	100	98–102		13,550	170	12,540	160	1,010	233	−5.1	68	49	

[a]Question marks denote possible anomalous points due to the reversed dates. Certainly anomalous points are deleted.

ensured that they encompassed the same core depth based on composite depths. The information on the width and weight of the planktonic and benthic foraminiferal samples is given in more detail in the Tables 1 and 2.

The samples were prepared and analyzed using standard procedures within the relevant accelerator mass spectrometry (AMS) laboratory. The AMS ^{14}C measurements were done at the Beta Analytic Laboratory, USA. The new radiocarbon results reported in this study include 26 planktonic samples and 33 benthic ones. Previous results are also summarized and discussed in combination with the new data.

In the modern ocean, the deep water "ventilation age" means the ratio of reservoir volume to the injection rate of new deep water, which could be provided by the difference in the ^{14}C to C ratio in the dissolved inorganic carbon (DIC) between surface water and deep water. In this study, radiocarbon age differences between coexisting benthic and planktonic foraminifera shells (B-P age) differ from ventilation ages in that they are referenced to the ^{14}C to C ratio in warm surface water rather than that in the appropriate polar surface water [*Broecker et al*., 2004b]. Thus, B-P age adopted and discussed here represents the apparent ventilation age of water masses rather than the true deep water ventilation age, reflecting the renewal process of deep water masses essentially. Radiocarbon activity ($\Delta^{14}C$) values of deep water, in which benthic foraminifera dwelled, were also calculated using the summary equation for initial $\Delta^{14}C$ of *Adkins and Boyle* [1997]:

$$\Delta^{14}C = \left(e^{-14C\ age/8033} / e^{-\ Cal\ age/8266} - 1\right) * 1000 \quad (1)$$

where 8033 and 8266 are the Libby and true mean lives of ^{14}C in years, respectively. Uncertainty estimates of $\Delta^{14}C$ values reflect the compounded analytical uncertainty of benthic and calendar ages, determined with the approach of a Monte Carlo simulation.

3.3. Stable Isotope and Faunal Analysis

Benthic foraminifera *C. wuellerstorfi* (shell size: >154 μm, 3–10 specimens, every 4 cm in Core MD05-2896 and 16 cm in Core MD05-2904 generally) were picked for stable isotope analysis, performed at the State Key Laboratory of Marine Geology, Tongji University, following the standard procedure described in *Cheng et al*. [2005]. *Uvigerina peregrina* (shell size: >400 μm, 3–5 specimens, every 8 cm) in Core MD05-2904 during the last deglaciation were also selected for the stable isotopic analysis because of fewer *C. wuellerstorfi* shells in sediment samples. Foraminiferal $\delta^{18}O$ and $\delta^{13}C$ were measured using a Finnigan modern analog technique 253 mass spectrometer equipped with an automatic carbonate preparation device (Kiel III). The isotopic results were converted into international Pee Dee Belemnite scale by the National Bureau of Standards 18 and 19. The standard deviation is ±0.07‰ for $\delta^{18}O$ and ±0.04‰ for $\delta^{13}C$, respectively.

Benthic foraminiferal fauna (shell size: >154 μm) from Core MD05-2904 were analyzed at every 32 cm (approximately equivalent to 1000 years' time resolution). *Uvigerina*, *Cibicidoides*, *Bulimina*, *Melonis*, *Astrononion*, and the total number of benthic foraminifera were counted in order to estimate the potential impact of benthic bioturbation and then provide further constraints on the reliability of radiocarbon data in combination with benthic foraminiferal $\delta^{18}O$ records.

3.4. Chronology

The age models of the studied cores were established based on planktic radiocarbon data by using the CALIB 7.0 program with the Marine13 calibration data set [*Reimer et al*., 2013]. The regional marine reservoir age (ΔR) is defined as the deviation of the local radiocarbon age from the globally averaged reservoir age (~400 years). The weighted average prebomb ΔR value of the SCS is -23 ± 52 years from known-age prebomb shells [*Southon et al*., 2002] and corals [*Dang et al*., 2004]. However, past marine reservoir ages may have changed significantly but are not well constrained. Over the past 7500 years, the weighted average ΔR values based on the records of fossil coral in the SCS exhibited evident fluctuations and amounted to 151 ± 85 years or even larger in the middle Holocene [*Yu et al*., 2006, 2010a, 2010b]. *Sarnthein et al*. [2007] discovered a suite of five ^{14}C plateaus at Core GIK17940 after plateau-tuning matching with those at Site 1002 in the Cariaco basin during the last deglaciation and revealed that deglacial reservoir values varied from 2200 to 900 years, significantly higher than the values at present and in the Holocene. However, the deglacial reservoir data in the SCS were not adopted in this study due to the following reasons: (1) the inconsistent offsets in reservoir age estimates imply unlikely variations in surface reservoir age in the low-latitude region over short time scales; (2) it is implausible that the surface reservoir age gets so large in the open air-sea system, if so the surface waters would likely fail to record atmospheric ^{14}C plateaus; (3) it seems that pseudo ^{14}C plateaus may result from rapid spikes in

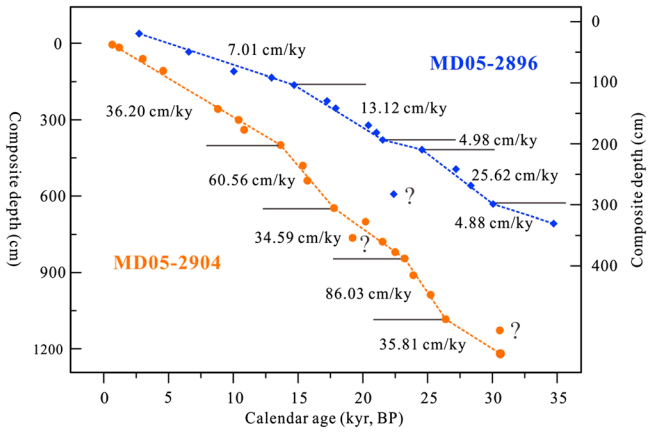

Figure 2. Plot of calendar age-depth with sedimentation rates (numbers beside the dashed lines) from two studied cores. Orange dots and blue diamonds denote radiocarbon dating points at depths from Cores MD05-2904 and MD05-2896, respectively. Question marks indicate the possible anomalous points.

hemipelagic sedimentation rate or subjective identification; and (4) there is no support of any ocean circulation models for so high surface reservoir age in the tropical ocean during the deglacial period. Therefore, in this study a constant reservoir age is chosen to determine calendar ages in the geologic past with generous error estimates. It is assumed $\Delta R = 200 \pm 300$ years in the past SCS, which covers both, modern values and estimates of past ΔR [*Southon et al.*, 2002; *Dang et al.*, 2004; *Yu et al.*, 2006; 2010]. It is noted that these errors also span the total range of glacial-inter glacial variability in the western Pacific reservoir ages estimated by the modeling study [*Butzin et al.*, 2005].

The estimates of calendar ages and errors ($\pm 1\sigma$) in both sites are shown in Figure 2 and Table 1. The age reconstructions are based on 21 and 16 radiocarbon measurements of *G. ruber* spanning over the last 30,000 ^{14}C years B.P. in MD05-2904 and MD05-2896, respectively. The average sedimentation rates are ~36 cm/kyr and ~7 cm/kyr in the Holocene, and ~46 cm/kyr and ~11 cm/kyr during the last glacial and deglacial period in the two cores, respectively. In Core MD05-2904, planktic ^{14}C ages and corresponding calendar dates reversed at two depths (705.5 cm and 763.5 cm) against the depth-age trends at certain sedimentation rates. However, it seems to be hard to determine either which point of them or both were anomalous exactly. Another point at the depth of 1127.5 cm in this site was also likely anomalous based on evidently negative B-P age (−1100 years) and extremely high sediment rate between 1127.5 cm and 1219.5 cm. The samples at these depths could be influenced by downslope transport because of the location near the continental slopes, rather than by bioturbation due to high sedimentation rates. One sample depth (282.5 cm) from Core MD05-2896 produced apparently anomalous ages out of stratigraphic order by more than their one sigma analytical uncertainty, probably affected by reworking material. Therefore, the radiocarbon results above mentioned are not included as age control points.

In order to further check the radiocarbon-based age models in these two locations, we compared the published δ^{18}O and Mg/Ca ratio of *G. ruber* previously based on planktonic ^{14}C dates using a linear interpolation in between the tie points since the last glacial period (Figures 3b and 3c). The curves of *G. ruber* δ^{18}O in both cores were well correlated with those of the East Asian stalagmite δ^{18}O records by documenting deglacial abrupt climate events (H1, B/A, and YD) [*Wang et al.*, 2001, 2005]. Moreover, sea surface temperature (SST) reconstructed from *G. ruber* Mg/Ca ratio in MD05-2904 indicated deglacial warming generally and no cooling in the YD interval, which matched the viewpoint that the YD did not induce a cooling but an arid episode from the previous study in the northern SCS [*Wang et al.*, 1999]. Therefore, it is believed that the chronological models derived from the planktonic ^{14}C data in both sites are reliable and precise.

Additionally, the new chronological models in the previous study from the SO50-37KL and V35-6 were reestablished with the above mentioned dating method employing updated CALIB 7.0 program with the Marine13 calibration data set [*Reimer et al.*, 2013] and the relatively wide range of ΔR (200 ± 300 years). These age models are also given in Table 1.

4. Results

4.1. The δ^{13}C Variation of Benthic Foraminifera

The δ^{13}C of *C. wuellerstorfi* in Core MD05-2904 and MD05-2896 and their three-point moving average curve (Figure 3e) display similar fluctuations in general, with minimum values during the Last Glacial Maximum

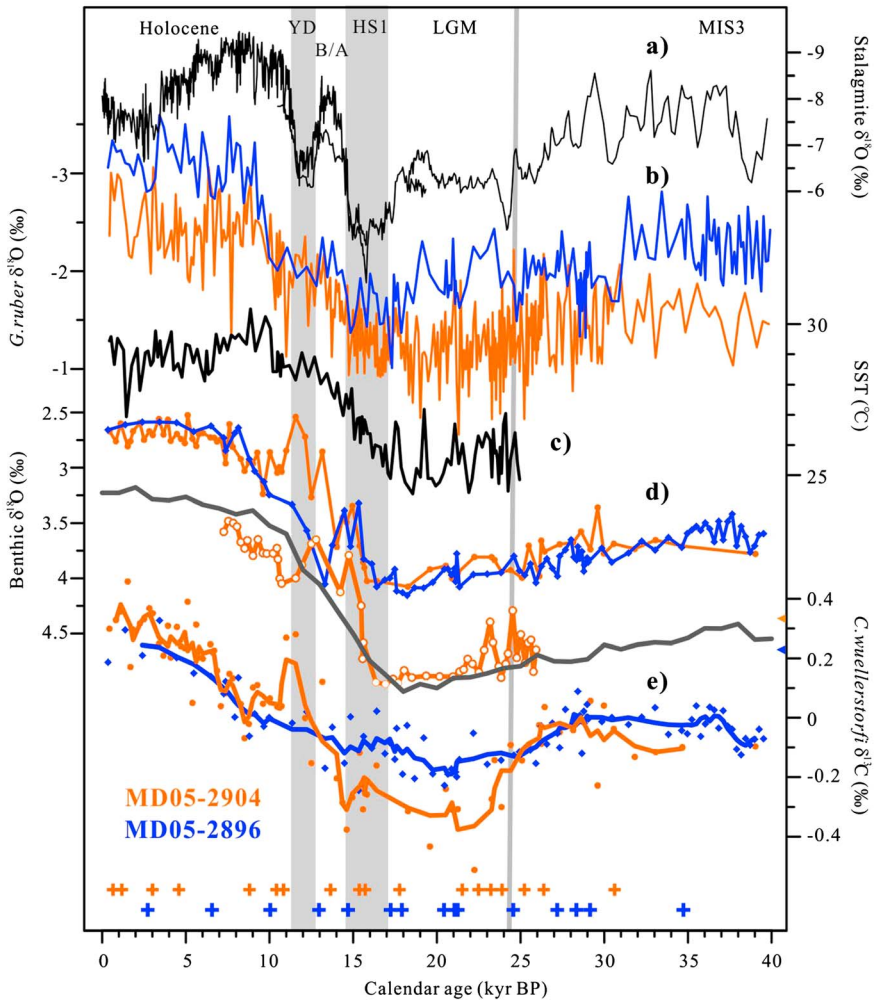

Figure 3. Comparison between planktic and benthic foraminiferal stable isotopic records over the past 40 kyr. Orange symbols and curves indicate the records from core MD05-2904 (solid circles for *C. wuellerstorfi* and open ones for *U. peregrina*), while blue ones show the counterparts from core MD05-2896. Lower crosses are the radiocarbon dating control points. YD, B/A, HS1, LGM, and MIS 3 denote Younger Dryas, Bolling/Allerod, Heinrich Stadial 1, Last Glacial Maximum and marine isotope stage 3, respectively. (a) East Asian Stalagmite δ^{18}O records [*Wang et al*., 2001, 2005]. (b) *G. ruber* δ^{18}O data of both cores after *Ge et al*. [2010] and *Tian et al*. [2010]. (c) Sea surface temperature based on *G. ruber* Mg/Ca ratio records in MD05-2904 [*Steinke et al*., 2011]. (d) Benthic foraminiferal δ^{18}O data in both cores. The black curve represents the LR04 stack [*Lisiecki and Raymo*, 2005]. (e) *C. wuellerstorfi* δ^{13}C records in both cores.

(LGM) and then an increasing trend toward the present. At the orbital time scale, the δ^{13}C values in the northern site decreased in average from ~ −0.08‰ in MIS3 to ~ −0.34‰ during the LGM, and then increased gradually through the deglaciation to ~0.33‰ in the late Holocene. Similarly, the southern δ^{13}C records exhibited a decline of ~0.07‰ from ~ −0.08‰ in MIS3 to ~ −0.15‰ during the LGM, and then a deglacial rise step by step until to ~0.23‰ in the late Holocene. Superimposed on this general trend, the short-term millennial excursions in δ^{13}C existed during the deglaciation. δ^{13}C showed two maxima in HS1 and the YD interval, interrupted by slightly low δ^{13}C values in the B/A time slice in both cores. There were also relatively negative δ^{13}C excursions in the early Holocene particularly in Core MD05-2904.

4.2. Evaluation of Radiocarbon Data Quality

Foraminiferal ^{14}C ages could be biased by dissolution, bioturbation, reworking and winnowing, which would influence the reliability and accuracy of ^{14}C dating [*Barker et al*., 2007; *Mekik*, 2014]. Modeling and ^{14}C records illustrate that dissolution could play a significant part in causing foraminiferal ^{14}C ages estimates biased to some extent [*Keir and Michel*, 1993; *Broecker et al*., 1991; *Barker et al*., 2007]. However, dissolution should not be

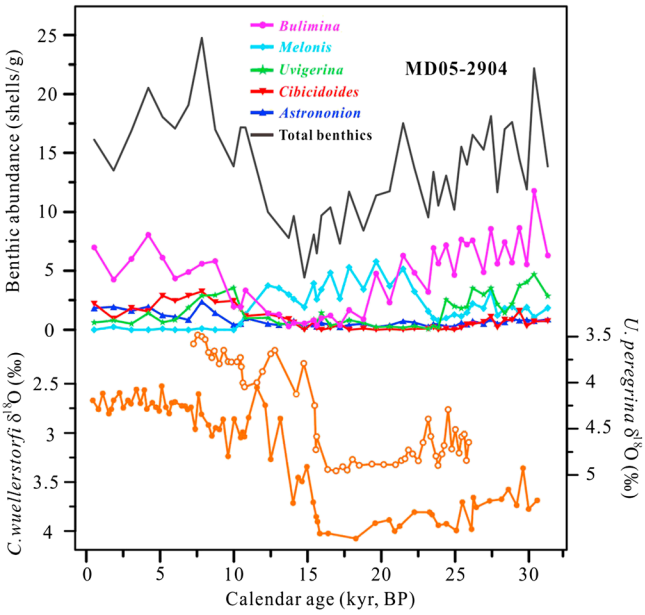

Figure 4. Benthic foraminiferal $\delta^{18}O$ and abundance records from Core MD05-2904. Benthic foraminiferal abundance data are as follows: purple dots and line, *Bulimina*; light blue prismatics and line, *Melonis*; green stars and line, *Uvigerina*; red triangles and line, *Cibicidoides*; blue inverted triangles and line, *Astrononion*; black line, total benthics. Orange solid and open circles indicate $\delta^{18}O$ points of *C. wuellerstorfi* and *U. peregrina* in this core, respectively.

regarded as a dominate factor on planktonic and benthic ^{14}C records in two studied cores. On the one hand, the modern calcite lysocline and com pensation depths are located at approximately 3000 m and 3800 m in the SCS, respectively. The depths were even deeper in the glacial period [*Thunell et al.*, 1992; *Miao et al.*, 1994]. These imply excellent carbonate preservation with little dissolution in both cores. On the other hand, the carbonate ion concentration ($[CO_3^{2-}]$) based on the proxies of foraminiferal weight differences and *C. wuellerstorfi* B/Ca ratio shows slight variations in the intermediate-depth (~2300 m) region of the Pacific since the last glacial period [*Broecker and Clark*, 2001; *Yu et al.*, 2010a, 2010b, 2013], probably indicative of minor changes in $[CO_3^{2-}]$ of the inflow into the deep SCS. Therefore, it is speculated that foraminiferal ^{14}C records were little impacted by dissolution in this study.

Major biases could be also created by homogeneous and heterogeneous bioturbation when coexisting planktic and benthic foraminiferal ^{14}C ages are applied for reconstructing the apparent ventilation ages [*Broecker et al.*, 1984; *Keigwin*, 2004]. It has been revealed that significant offsets of the measured ^{14}C between different species mainly occurred for lower rates of sediment accumulation (≤3 cm/kyr) [*Barker et al.*, 2007]. Due to the high sedimentation rates in Core MD05-2904 (Figure 2), foraminiferal ^{14}C measurements in this site should have little influence by the homogeneous bioturbation. The absolute abundances of benthic foraminifera (>154 μm) in this core approximately amounted to 15 ± 5 shells/g, 10 ± 3 shells/g, and 20 ± 5 shells/g in average during the last glaciation, the deglaciation and the Holocene, respectively, showing relatively stable fluctuation without abnormal spikes since the last glacial period (Figure 4). This indicates that the biases from the benthic foraminiferal abundance should be minimal. Benthic foraminiferal abundance data in Core MD05-2896 are not available. However, because both the planktonic and benthic foraminiferal ^{14}C data except those at the depth of 282.5 cm are in accordance with normal stratigraphic order within their one-sigma analytical uncertainty without abnormal sedimentation rates emerging, it seems that bioturbation does not have a strong influence on the ^{14}C records in Core MD05-2896.

In addition, benthic foraminiferal stable isotopic curves could help to determine the influence of reworked shells which may bias the radiocarbon measurments. The normal benthic $\delta^{18}O$ and $\delta^{13}C$ records in the two studied cores (Figure 3) reduce the possibility of reworked materials. However, results from one sample depth in MD05-2896 (282.5 cm) and three depths (844.5 cm, 910.5 cm, and 1127.5 cm) exhibit negative benthic-planktic ages, implying that the deep water reservoir age is younger compared with surface water which is a physically implausible $\Delta^{14}C$ relationship. One of the possible causes for these anomalous results is the incorporation of reworked materials. Downslope transport of sediments or planktonic foraminifera (e.g., *G. ruber*) from the previous deposits could bring reworked material carrying the false signal and resulting in negative benthic-planktic ages. Another possibility is sediment focusing. Sediment redistribution is likely to cause heavier benthics to remain in situ, and newly formed fragments and arriving lighter planktics to be winnowed away, which would alter the true benthic-planktic ages [*Broecker et al.*, 2006; *Mekik*, 2014]. Furthermore, more than one mechanism could be at play possibly, such as a combination of reworking, winnowing, and/or bioturbation.

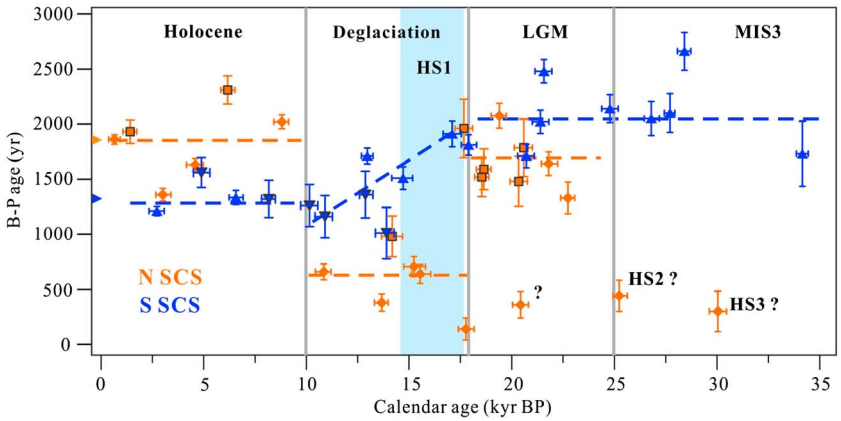

Figure 5. The B-P ages of the SCS since the last glacial period. Orange marks denote the deep ventilation ages in the northern basin from Cores MD05-2904 (diamonds) and SO50-37KL (squares with black borders), while blue symbols indicate those in the southern basin from Cores MD05-2896 (regular triangles) and V35-6 (inverted triangles with black borders). Here the new chronological framworks of Cores SO50-37KL and V35-6 [*Broecker et al*., 1990; *Sarnthein et al*., 2007; *Andree et al*., 1986; *Broecker et al*., 2006] (Table 2) are based on selected data points without reworked foraminiferal shells. Question marks denote low B-P values likely anomalous during HS2 and HS3 from Core MD05-2904. Error bars represent one standard deviation ($\pm 1\sigma$). Light blue bar indicates HS1. Horizontal dashed lines indicate the average values for the Holocene, deglaciation and glaciation intervals in the northern (orange) and southern (blue) SCS, respectively. The triangles next to the vertical axis display the respective average ventilation ages in the late Holocene.

Therefore, those points with age reversal (Table 1) or negative benthic-planktic ages (Table 2) in both cores are not included and interpreted in the following discussion. In general, the radiocarbon data from both cores are regarded reliable and appropriate for reconstruction of past changes in deep water properties and related oceanic processes.

As discussed previously based on *Broecker et al*. [2006], it was speculated that addition of reworked materials likely caused the large average age difference of ~890 years between coexisting planktic *Pulleniatina obliquiloculata* and *Globigerinoides sacculifer* in Core V35-5, in contrast with those of ~190 years and ~120 years in Core V35-6 and SO50-37KL, respectively. Because the robust species (*P. obliquiloculata*) live deeper in the water column than the fragile species (*G. sacculifer*), the difference in ^{14}C to C ratio in the DIC of the water in which they formed can at most produce a few hundred years age difference. Thus, the ^{14}C records in V35-6 and SO50-37KL rather than V35-5 appear to be normal so that they could be combined to reconstruct the apparent ventilation ages of deep water in the SCS.

4.3. Deep Water Ages in the SCS

Apparent ventilation ages (B-P ages) have displayed significant and distinct features between the northern and southern SCS since the last glacial period (Figure 5). It should be noted that in this study the new B-P records from Cores MD05-2904 and MD05-2896 have been drawn and discussed together with the published data based on the updated age models from Cores SO50-37KL [*Broecker et al*., 1990; *Sarnthein et al*., 2007] and V35-6 [*Broecker et al*., 1988, 1990; *Andree et al*., 1986] bathed in the SCS deep water. B-P ages in the northern SCS were ~1600 years during the LGM, which was comparable to the present value or a little younger within the uncertainties. Notably, there existed young deep water of ~500 years old at ~25.2 kyr B.P. and ~30.6 kyr B.P., which might corresponded to the newly formed North Pacific deep water in the severe stadial episodes during the last glacial period [*Rella et al*., 2012; *Horikawa et al*., 2010]. Another point with B-P age of 360 years at ~20.1 kyr B.P. was probably due to above mentioned stratigraphic disturbance. B-P ages in the southern SCS averaged ~2050 years with minor fluctuations during the last glaciation. The average gradient between the southern and northern SCS deep water ages approximately equaled to ~400 years in the glacial period (Figure 5 and Table 2).

During the last deglaciation (18–10 kyr B.P.), the deep water $\Delta^{14}C$ changes both in the northern and southern SCS display a gradual reduction generally, comparable with the previous atmospheric curves (IntCal13). Deglacial B-P ages in the northern SCS decreased to ~670 years in average from the glacial level, while they exhibited a declined trend approximately from ~2000 years at the end of LGM to ~1250 years until the late

deglaciation in the southern SCS. The deglacial north-south ventilation gradient is estimated to be ~800 years in average (Table 2). During the Mystery Interval specifically, there is no sign for remarkable intrusions of anomalously ^{14}C-depleted water masses at these northern and southern sites. The average deep water Δ^{14}C values of northern (100‰) and southern (−19.4‰) SCS appeared not to be remarkably depleted compared with the Baja California intermediate water records during this interval [*Marchitto et al*., 2007].

Since the early Holocene, the north-south gradient of deep water age reversed completely in the SCS. The B-P ages amount to ~1850 years and ~1350 years in average through the whole Holocene in the northern and southern SCS, respectively, with a gradient of ~500 years (Figure 5). Along the flow path, the deep water became younger from north to south in the SCS during the Holocene, probably due to strong vertical diffusion when flowing southward. This is in contrast with the conditions during the last glacial and deglacial periods, clearly indicating different characteristics of deep circulation. Therefore, the ^{14}C records from these cores in the SCS have documented significant changes in the deep oceanic processes since the last glacial period.

5. Discussion

5.1. Changes in Deep Oceanic Processes Within the SCS

The deep apparent ventilation ages provide major information on the source of water masses and the deep water renewal conditions. The deep water renewal within the SCS could be assessed by analyzing the gradient of deep water apparent ventilation ages between the northern and southern SCS since the last glacial period. The south-north gradient might be influenced by internal oceanic processes involving the advection intensity and other water mass mixing such as the downwelling of intermediate water or the upwelling of aged deep water. Theoretically, the deep water ages should be older in the southern SCS than in the northern part, because the Luzon Strait located in the northeastern SCS is the only gateway for the SCS deep water and within the SCS basin the deep water counterclockwise flows from north to south [*Qu et al*., 2006]. However, it is not the case in the Holocene. Instead, an opposite south-north gradient of deep ventilation ages was found: the deep water became younger from north to south in the SCS during the Holocene. According to the modern investigations, the modern SCS deep water has a fast renewal rate related with vigorous vertical diffusion, deep upwelling and advection [*Tian et al*., 2009; *Qu et al*., 2006; *Dai et al*., 2013]. Therefore, it is inferred that the southward advection of water masses together with enhanced vertical mixing between the intermediate and deep layers in the basin could have resulted in younger southern deep water. Based on the study of the modern carbon cycle, the SCS is considered as a weak CO_2 source overall [*Chai et al*., 2009; *Chen et al*., 2006]. It is believed that the intrabasin oceanic processes such as vigorous diapycnal mixing and deep upwelling may play a crucial role in releasing excessive CO_2 from the deep ocean to the atmosphere at present [*Dai et al*., 2013]. According to Figure 5, this mechanism of pumping deep water carbon up to the sea surface existed likely throughout the Holocene in the SCS.

However, during the LGM and the last deglaciation, the SCS deep water became older from north to south, displaying a trend opposite with that of the Holocene (Figure 5). It is inferred that the glacial positive south-north gradient in deep water ages could indicate the significantly decreased deep renewal rate at that time compared to the Holocene. Based on the modern observations, the deep inflow from the Pacific into the SCS is primarily driven by a persistent baroclinic pressure gradient across the Luzon Strait, sustained by modern strong deep diapycnal mixing in the region [*Zhao et al*., 2014; *Qu et al*., 2006]. Probably, the reduced glacial deep vertical mixing and advection would have brought about a weaker baroclinic pressure gradient across the Luzon Strait and thus weakened inflow and renewal. In addition, the relatively reduced glacial intrabasin renewal largely led to oxygen-deficient bottom conditions consistent with the middepth deposition of organic-rich sediments and benthic δ^{13}C depletion to some extent during the last glacial in the southern SCS [*Jian et al*., 1999].

The intrabasin deep renewal of the SCS was improved since the middle-late deglaciation. In addition to the influence of increased deep ventilation in the western Pacific [*Broecker et al*., 2008] (Figure 6), there is also a significant local factor of internal enhanced vertical mixing and advection in the deep SCS. Overall, the intrabasin deep water renewal of the SCS was weak during the LGM and the last deglaciation based on the remarkably increased south-north gradient of 600 years and 800 years, respectively, and then notably en hanced during the Holocene inferred from the reversed gradient (Figure 5). In general, during the LGM the

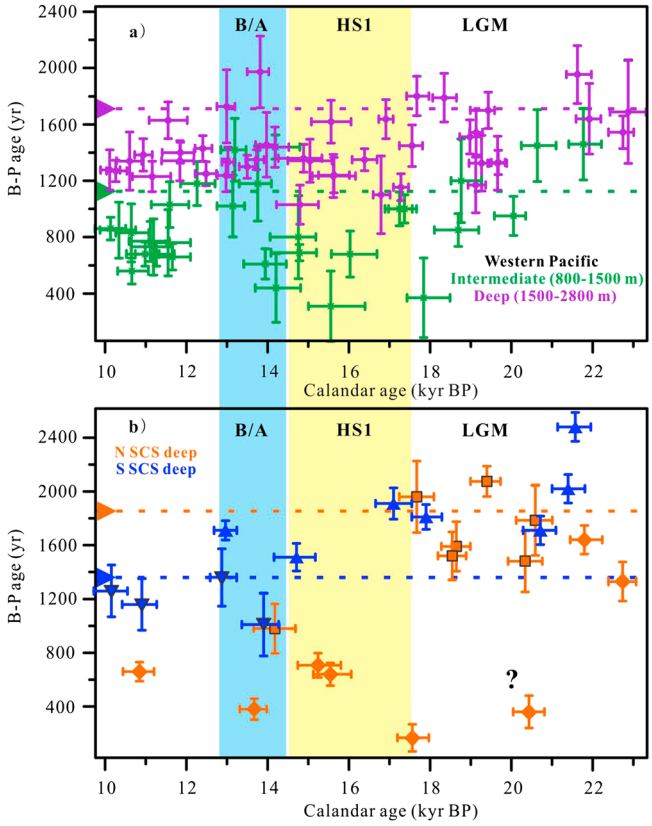

Figure 6. Comparison of B-P ages between the SCS and the western Pacific region during the deglacial interval. (a) Compilation of intermediate (green marks) [*Ahagon et al.*, 2003; *Duplessy et al.*, 1989; *Sagawa and Ikehara*, 2008] and deep (purple symbols) [*Broecker et al.*, 2004a, 2008; *Minoshima et al.*, 2007; *Sarnthein et al.*, 2007; *Okazaki et al.*, 2012] ventilation variations from available radiocarbon documents in the western Pacific. The calendar ages are converted from radiocarbon ages with Calib 7.0 using contant reservoir age of $\Delta R = 500 \pm 300$ years, 100 ± 200, and 160 ± 150 yr in the subartic and mid-latitude and low-latitude western Pacific, respectively [*Okazaki et al.*, 2010]. (b) Deep ventilation ages in the SCS. Orange marks denote the deep ventilation ages from Cores MD05-2904 (diamonds) and SO50-37KL (squares with black borders), while blue symbols indicate those from Cores MD05-2896 (regular triangles) and V35-6 (inverted triangles with black borders). Triangle symbols next to the vertical axis display the levels of intermediate or deep apparent ventilation age at present (the western Pacific) or in the late Holocene (the SCS) [*Key et al.*, 2004; *Broecker et al.*, 2004b]. Error bars represent one standard deviation ($\pm 1\sigma$). Light orange and blue bars indicate HS1 and the B/A interval, respectively.

SCS deep water renewal was relatively weakened and thus the SCS probably became a sink of atmospheric CO_2, not a weak CO_2 source like at present [*Dai et al.*, 2013] and in the Holocene.

5.2. Enhanced Influence of NPDW During the Deglaciation

The averaged B-P age in the northern SCS was relatively younger in the last deglaciation compared with those in the Holocene and the LGM (Figure 5), with three possible explanations: (1) remarkably strengthened vertical mixing between the upper and deep waters in the SCS, (2) intrusion of better ventilated southern sourced waters, and (3) enhanced input of the newly formed deep water from the North Pacific because of the shortened transport distance to the SCS compared with the southern sourced aged deep water.

The first option seems unlikely because the vertical mixing occurs mainly in the intermediate and deep waters of the SCS [*Qu et al.*, 2006; *Tian et al.*, 2009], and that the deglacial deep vertical mixing was relatively weakened compared with that in the Holocene based on the south-north gradient of B-P age in the SCS. The second explanation is also considered as an inappropriate option. The deep apparent ventilation ages kept near constant in the western equatorial Pacific and increased by ~1000 years in the northeast Pacific during the deglaciation compared to the mod ern values, respectively [*Broecker et al.*, 2008; *Lund et al.*, 2011]. These findings would not support obviously better ventilated southern sourced waters into the deep Pacific. Therefore, the third explanation is the most likely.

The water mass structure in the North Pacific made fundamental transformation from a glacial stratification mode, across the deglacial ventilation mode locally, to an interglacial upwelling mode [*Herguera et al.*, 2010; *Okazaki et al.*, 2010, 2012; *Max et al.*, 2013]. The glacial North Pacific included two different water masses mainly based on nutrient proxy $\delta^{13}C$: well-ventilated and nutrient-depleted glacial North Pacific intermediate water (GNPIW) above ~2000 m and less-ventilated and nutrient-enriched deep water below ~2000 m [*Keigwin*, 1998; *Matsumoto et al.*, 2002]. The upper nutrient-depleted water mass probably involved a process combining the northern sourced water mass newly formed in the high-latitude North Pacific with the southern sourced modified glacial North Atlantic Intermediate Water (GNAIW) reaching the Pacific Ocean via the Southern Ocean [*Boyle*, 1992; *Matsumoto and Lynch-Stieglitz*, 1999; *Matsumoto et al.*, 2002].

It had been inferred from microfossil and geochemical evidence that GNPIW was likely generated in the Bering Sea during the glacial cold period [*Rella et al*., 2012; *Horikawa et al*., 2010; *Ohkushi et al*., 2003]. However, the apparent ventilation ages of the western Pacific intermediate deep waters and the northern SCS deep water during the LGM were equivalent to or older than corresponding modern values, respectively, reflecting that the possible North Pacific deep water formation did not exert a dominant influence on the whole of the North Pacific during the glacial (Figure 6). It might be expected that the glacial deep water in the middle-low-latitude northwest Pacific and the marginal SCS was influenced largely by the penetration of southern sourced modified deep water from the Southern Ocean overwhelming the influence of northern sourced North Pacific deep water (also regarded as GNPIW herein) generally. The remarkable influence of the southern sourced aged Pacific deep water during the LGM in the SCS was also reflected in the occurrence of benthic foraminifer *Favocassidulina favus*, indicator of the modern Pacific Bottom Water, which was not found in the SCS since the last deglaciation [*Jian and Wang*, 1997].

During the middle-late H1 in the early deglaciation, deep water formed powerfully in the high-latitude North Pacific extending to a depth of even more than ~2500–3000 m and flowed southward along the western margin of the Pacific based on a compilation of radiocarbon records and modeling simulations, compared to the almost shutdown of the NADW generation and the Atlantic meridional overturning circulation [*Sarnthein et al*., 2007, 2011; *Okazaki et al*., 2010; *Rae et al*., 2014; *Menviel et al*., 2012; *McManus et al*., 2004]. The deep water formation and penetration downward may extend to the late deglaciation with variable strength according to the records of strong ventilation and upper vertical mixing from the subarctic eastern and western deep North Pacific [*Gebhardt et al*., 2008; *Sarnthein et al*., 2007]. The deglacial ventilation ages in the western North Pacific were overall lower than those in the LGM and Holocene (Figure 6), which showed distinctive characteristics compared with those in the northeast Pacific [*Lund et al*., 2011]. The west-east differences could be driven by the distinct expanding intensity of newly formed North Pacific deep water with more enhanced influence along the western Pacific. Moreover, the northwestern Pacific intermediate water appeared to display greater ventilation ages during the B/A interval compared to that of the regional deep water, implying different water mass sources for the intermediate and deep waters [*Minoshima et al*., 2007] (Figure 6). The deep water ^{14}C records of Core MD05-2904 together with other data in the western Pacific [*Gebhardt et al*., 2008; *Sarnthein et al*., 2007; 2011] provide strong evidence for the increased deep water ventilation in the region and enhanced influence of newly formed North Pacific deep water on the low-latitude regions during the deglaciation.

In the Holocene, the inflow deep water in the northern SCS averaged ~1850 years old, possibly indicating the recovery of dominant influence of southern sourced deep water (UCDW) on the low-latitude western Pacific and the SCS. At present, the deep water flows into the North Pacific from the south, and then upwells to middepth and returns southward as the Pacific Deep Water (NPDW) [*Schmitz*, 1996]. Above the NPDW, the North Pacific Intermediate Water (NPIW) defined as the salinity minimum at depths of 300–800 is formed in the high-latitude northwestern Pacific, whose origin is thought to locate in the Sea of Okhotsk [*Yasuda*, 1997]. Our records exclude that NPIW overspreads significantly downward and southward to the deep ocean in the low-latitude western Pacific and the SCS during the entire Holocene unlike during the last deglaciation. In combination with modern observations [*Kawabe and Fujio*, 2010; *Chang et al*., 2010], it may be regarded that southern sourced UCDW has a major impact on the low-latitude western Pacific and flow dominantly into the deep SCS during the Holocene. Therefore, the modern ocean circulation pattern was eventually established in the early Holocene [*Negre et al*., 2010].

5.3. Implications for the Release of Old Deep Water Carbon

During the Mystery Interval, anomalously ^{14}C-depleted intermediate water has been found in the eastern Pacific and northern Arabian Sea [*Marchitto et al*., 2007; *Stott et al*., 2009; *Bryan et al*., 2010], supporting the existence of a glacial-age ^{14}C-deficient isolated deep reservoir whose demise might account for the observed atmospheric ^{14}C decline [*Broecker and Clark*, 2010]. However, it is still unclear where the ^{14}C-depleted source came from and how the ^{14}C-depleted water masses transported from the deep to the upper ocean and the atmosphere mechanically. So far, there is no evidence for extremely ^{14}C-depleted water mass in the SCS as the "dead end" of deep circulation in the Pacific, although its deep water ventilation decreased during the LGM. The deep water $\Delta^{14}C$ in the SCS was approximately 90‰ during the LGM, similar to those in the western Pacific [*Broecker et al*., 2008; *Okazaki et al*., 2012]. The compiled $\Delta^{14}C$ records of immediate and deep waters in the

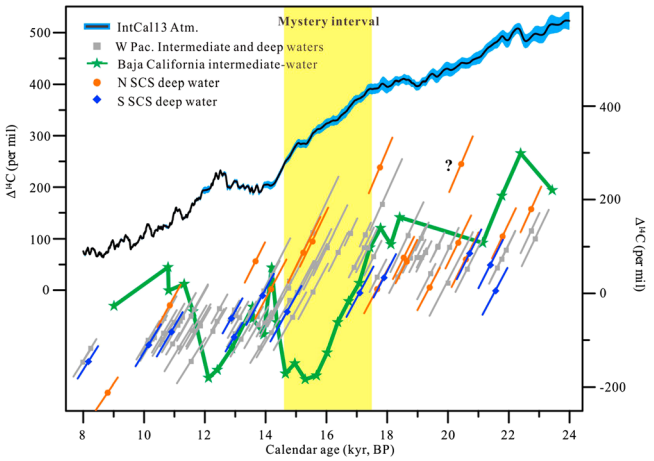

Figure 7. Time series of deglacial deep $\Delta^{14}C$ in the SCS (orange circles and blue diamonds, respectively) and western Pacific (grey squares). The compiled $\Delta^{14}C$ in the western Pacific are calculated from the records introduced in Figure 6a. $\Delta^{14}C$ data of atmosphere (black line with blue bands) and intermediate water in Baja Califonia (green line with stars) are also shown [*Reimer et al*., 2013; *Marchitto et al*., 2007]. Error bars are determined with the method of a Monte Carlo simulation. Light orange bar indicates the Mystery Interval. Question mark denotes anomalous positive $\Delta^{14}C$ value in Core MD05-2904.

western North Pacific indicate that this region was not a significant ^{14}C-depleted reservoir during glacial times (Figure 7). Also, there is no evidence for such an old abyssal carbon reservoir in the northeastern and equatorial Pacific [*Broecker and Clark*, 2010; *Lund et al*., 2011]. If a glacial "Mystery Reservoir" had existed in the deep ocean, the Southern Ocean would have been assumed to provide ^{14}C-depleted water masses [*Burke and Robinson*, 2012]. During the Mystery Interval, the widespread increase in upwelling of the Southern Ocean and the coeval onset of downwelling of North Pacific deep and intermediate waters marked the fundamental transformation of deep ocean circulation and thus led to massive CO_2 degassing from the deep ocean to the atmosphere [*Köhler et al*., 2005; *Sarnthein et al*., 2007].

Hain et al. [2011] pointed out that the middepth $\Delta^{14}C$ anomalies did not record basin-scale changes but local phenomena. There are still only scattered records of $\Delta^{14}C$ anomalies based on the immediate water from the low-latitude eastern Pacific, northern Arabian Sea, and South Iceland Rise [*Marchitto et al*., 2007; *Stott et al*., 2009; *Bryan et al*., 2010; *Sarnthein et al*., 2007], and deep water from the high-latitude northeast Atlantic Ocean [*Thornalley et al*., 2011] during the Mystery Interval. Our results have provided further evidence that there was no sign for remarkable intrusions of anomalously ^{14}C-depleted water masses into the deep western North Pacific and the SCS during the Mystery Interval (Figure 7), consistent with the previous observations based on other equatorial and middle-high-latitude sites in the western Pacific [*Sarnthein et al*., 2011; *Okazaki et al*., 2010, 2012; *Broecker et al*., 2008]. Instead, in the western North Pacific, the deep water formation and southward extension may have played an even more significant role in the local middepth $\Delta^{14}C$ values [*Okazaki et al*., 2010, 2012], compared with the influence of southern sourced aged Pacific deep water from the Southern Ocean.

6. Conclusions

In this study, we have reconstructed the deep water apparent ventilation ages (B-P ages) and $\Delta^{14}C$ records since the last glacial period from two cores with high sedimentation rates in the northern and southern SCS, respectively. During the Holocene, the deep water became younger from north (~1850 years) to south (~1280 years) in the SCS along the deep water flow path due to strong deep renewal involving enhanced vertical mixing and advection. However, during the last glacial period and deglaciation the deep water ventilation ages were relatively older in the southern (~2050 years and ~1460 years, respectively) than in the northern (~1600 years and ~670 years, respectively) SCS, indicating that the deep renewal was weakened as a result of reduced vertical mixing and advection during this period.

Comparison of regional apparent ventilation ages indicates the primary influence of the southern sourced aged Pacific deep water to the SCS and low-latitude western Pacific during the last glacial period. This was also reflected in the occurrence of benthic foraminifer *Favocassidulina favus*, indicator of the modern Pacific Bottom Water, in the SCS during this period [*Jian and Wang*, 1997]. During the last deglaciation the northern SCS deep water was the youngest, significantly different from the observed $\Delta^{14}C$ decrease in the middepth core near Baja California during the Mystery Interval (17.5–14.5 kyr B.P.). This further supports no remarkable intrusion of anomalously ^{14}C-depleted deep water into the low-latitude western Pacific and the

SCS during the last deglaciation, consistent with other observations from the western equatorial Pacific [*Broecker et al*., 2008; *Okazaki et al*., 2012]. On the contrary, our records support the existence of relatively younger deep water such as the northern sourced newly formed North Pacific deep water during the last deglaciation [*Okazaki et al*., 2010; *Sarnthein*, 2011]. Therefore, the deep water of the low-latitude western Pacific and SCS has experienced significant changes, which could affect the carbon cycle during the glacial cycles.

Acknowledgments

All samples used in this study were from the Sino-French joint cruise MD147/MARCO POLO-IMAGES XII of French R/V *Marion Dufresne* in 2005. The authors thank Xinrong Cheng for the stable isotopic analysis, Michael Sarnthein, Haiyan Jin, and Enqing Huang for discussions, and two anonymous reviewers for their constructive comments. The complete data produced by this study are available via Anonymous FTP from mlab.tongji.edu.cn or upon request form jian@tongji.edu.cn. This study was supported by the National Natural Science Foundation of China (grants 91028004 and 41023004), the State Oceanic Administration of China, and the International Associated Laboratories (LIA) project "Monsoon, Ocean and Circulation (MONOCL)."

References

Adkins, J. F., and E. A. Boyle (1997), Changing atmospheric $\Delta^{14}C$ and the record of deep water paleoventilation ages, *Paleoceanography*, *12*(3), 337–344, doi:10.1029/97PA00379.

Ahagon, N., K. Ohkushi, M. Uchida, and T. Mishima (2003), Mid-depth circulation in the northwest Pacific during the last deglaciation: Evidence from foraminiferal radiocarbon ages, *Geophys. Res. Lett.*, *30*(21), 2097, doi:10.1029/2003GL018287.

Andree, M., et al. (1986), Limits on the ventilation rate for the deep ocean over the last 12000 years, *Clim. Dyn.*, *1*(1), 53–62.

Barker, S., W. Broecker, E. Clark, and I. Hajdas (2007), Radiocarbon age offsets of foraminifera resulting from differential dissolution and fragmentation within the sedimentary bioturbated zone, *Paleoceanography*, *22*, PA2205, doi:10.1029/2006PA001354.

Boyle, E. A. (1992), Cadmium and delta ^{13}C paleochemical ocean distributions during the stage 2 glacial maximum, *Annu. Rev. Earth Planet. Sci.*, *20*, 245–287.

Broecker, W., and S. Barker (2007), A 190‰ drop in atmosphere's $\Delta^{14}C$ during the "Mystery Interval" (17.5 to 14.5 kyr), *Earth Planet. Sci. Lett.*, *256*(1–2), 90–99.

Broecker, W., and E. Clark (2010), Search for a glacial-age ^{14}C-depleted ocean reservoir, *Geophys. Res. Lett.*, *37*, L13606, doi:10.1029/2010GL043969.

Broecker, W., A. Mix, M. Andree, and H. Oeschger (1984), Radiocarbon measurements on coexisting benthic and planktic foraminifera shells: Potential for reconstructing ocean ventilation times over the past 20 000 years, *Nucl. Instrum. Methods Phys. Res., Sect. B*, *5*(2), 331–339.

Broecker, W., S. Barker, E. Clark, I. Hajdas, G. Bonani, and L. Stott (2004a), Ventilation of the glacial deep Pacific Ocean, *Science*, *306*(5699), 1169–1172.

Broecker, W., S. Barker, E. Clark, I. Hajdas, and G. Bonani (2006), Anomalous radiocarbon ages for foraminifera shells, *Paleoceanography*, *21*, PA2008, doi:10.1029/2005PA001212.

Broecker, W., E. Clark, S. Barker, I. Hajdas, G. Bonani, and E. Moreno (2007), Radiocarbon age of late glacial deep water from the equatorial Pacific, *Paleoceanography*, *22*, PA2206, doi:10.1029/2006PA001359.

Broecker, W., E. Clark, and S. Barker (2008), Near constancy of the Pacific Ocean surface to mid-depth radiocarbon-age difference over the last 20 kyr, *Earth Planet. Sci. Lett.*, *274*(3–4), 322–326.

Broecker, W. S. (1982), Ocean chemistry during glacial time, *Geochim. Cosmochim. Acta*, *46*(10), 1689–1705.

Broecker, W. S., and E. Clark (2001), Glacial-to-Holocene redistribution of carbonate ion in the deep sea, *Science*, *294*(5549), 2152–2155.

Broecker, W. S., M. Andree, G. Bonani, W. Wolfli, H. Oeschger, M. Klas, A. Mix, and W. Curry (1988), Preliminary estimates for the radiocarbon age of deep water in the glacial ocean, *Paleoceanography*, *3*(6), 659–669, doi:10.1029/PA003i006p00659.

Broecker, W. S., T.-H. Peng, S. Trumbore, G. Bonani, and W. Wolfli (1990), The distribution of radiocarbon in the glacial ocean, *Global Biogeochem. Cycles*, *4*(1), 103–117, doi:10.1029/GB004i001p00103.

Broecker, W. S., M. Klas, E. Clark, G. Bonani, S. Ivy, and W. Wolfli (1991), The influence of $CaCO_3$ dissolution on core top radiocarbon ages for deep-sea sediments, *Paleoceanography*, *6*(5), 593–608, doi:10.1029/91PA01768.

Broecker, W. S., E. Clark, I. Hajdas, and G. Bonani (2004b), Glacial ventilation rates for the deep Pacific Ocean, *Paleoceanography*, *19*, PA2002, doi:10.1029/2003PA000974.

Bryan, S. P., T. M. Marchitto, and S. J. Lehman (2010), The release of ^{14}C-depleted carbon from the deep ocean during the last deglaciation: Evidence from the Arabian Sea, *Earth Planet. Sci. Lett.*, *298*(1–2), 244–254.

Burke, A., and L. F. Robinson (2012), The Southern Ocean's role in carbon exchange during the last deglaciation, *Science*, *335*(6068), 557–561.

Butzin, M., M. Prange, and G. Lohmann (2005), Radiocarbon simulations for the glacial ocean: The effects of wind stress, Southern Ocean sea ice and Heinrich events, *Earth Planet. Sci. Lett.*, *235*(1–2), 45–61.

Chai, F., G. Liu, H. Xue, L. Shi, Y. Chao, C.-M. Tseng, W.-C. Chou, and K.-K. Liu (2009), Seasonal and interannual variability of carbon cycle in South China Sea: A three-dimensional physical-biogeochemical modeling study, *J. Oceanogr.*, *65*(5), 703–720.

Chang, Y.-T., W.-L. Hsu, J.-H. Tai, T. Tang, M.-H. Chang, and S.-Y. Chao (2010), Cold deep water in the South China Sea, *J. Oceanogr.*, *66*(2), 183–190.

Chao, S.-Y., P.-T. Shaw, and S. Y. Wu (1996), Deep water ventilation in the South China Sea, *Deep Sea Res., Part I*, *43*(4), 445–466.

Chen, C.-T. A., S.-L. Wang, B.-J. Wang, and S.-C. Pai (2001), Nutrient budgets for the South China Sea basin, *Mar. Chem.*, *75*(4), 281–300.

Chen, C.-T. A., S.-L. Wang, W.-C. Chou, and D. D. Sheu (2006), Carbonate chemistry and projected future changes in pH and $CaCO_3$ saturation state of the South China Sea, *Mar. Chem.*, *101*(3–4), 277–305.

Cheng, X., B. Huang, Z. Jian, Q. Zhao, J. Tian, and J. Li (2005), Foraminiferal isotopic evidence for monsoonal activity in the South China Sea: A present-LGM comparison, *Mar. Micropaleontol.*, *54*(1–2), 125–139.

Dai, M., Z. Cao, X. Guo, W. Zhai, Z. Liu, Z. Yin, Y. Xu, J. Gan, J. Hu, and C. Du (2013), Why are some marginal seas sources of atmospheric CO_2?, *Geophys. Res. Lett.*, *40*, 2154–2158, doi:10.1002/grl.50390.

Dang, P. X., T. Mitsuguchi, H. Kitagawa, Y. Shibata, and T. Kobayashi (2004), Marine reservoir correction in the south of Vietnam estimated from an annually-banded coral, *Radiocarbon*, *46*(2), 657–660.

Duplessy, J.-C., N. J. Shackleton, R. K. Matthews, W. Prell, W. F. Ruddiman, M. Caralp, and C. H. Hendy (1984), ^{13}C Record of benthic foraminifera in the last interglacial ocean: Implications for the carbon cycle and the global deep water circulation, *Quat. Res.*, *21*(2), 225–243.

Duplessy, J. C., M. Arnold, E. Bard, A. Juillet-Leclerc, N. Kallel, and L. Labeyrie (1989), AMS ^{14}C study of transient events and of the ventilation rate of the Pacific intermediate water during the last deglacial, *Radiocarbon*, *31*(3), 493–502.

Emery, W. (2001), Water types and water masses, *Encycl. Ocean Sci.*, *6*, 3179–3187.

Galbraith, E. D., S. L. Jaccard, T. F. Pedersen, D. M. Sigman, G. H. Haug, M. Cook, J. R. Southon, and R. Francois (2007), Carbon dioxide release from the North Pacific abyss during the last deglaciation, *Nature*, *449*(7164), 890–893.

Garcia, H. E., R. A. Locarnini, T. P. Boyer, J. I. Antonov, O. K. Baranova, M. M. Zweng, and D. R. Johnson (2010), *World Ocean Atlas 2009, Volume 3: Dissolved Oxygen, Apparent Oxygen Utilization, and Oxygen Saturation*, NOAA Atlas NESDIS, vol. 70, edited by S. Levitus, 344 pp., U.S. Government Printing Office, Washington, D. C.

Ge, H., Q. Li, X. Cheng, H. Zheng, and J. He (2010), Late Quaternary high resolution monsoon records in planktonic stable isotopes from northern South China Sea, *Earth Sci. J. China Univ. Geosci.*, *35*(4), 515–525.
Gebhardt, H., M. Sarnthein, P. M. Grootes, T. Kiefer, H. Kuehn, F. Schmieder, and U. Röhl (2008), Paleonutrient and productivity records from the subarctic North Pacific for Pleistocene glacial terminations I to V, *Paleoceanography*, *23*, PA4212, doi:10.1029/2007PA001513.
Hain, M. P., D. M. Sigman, and G. H. Haug (2011), Shortcomings of the isolated abyssal reservoir model for deglacial radiocarbon changes in the mid-depth Indo-Pacific Ocean, *Geophys. Res. Lett.*, *38*, L04604, doi:10.1029/2010GL046158.
Herguera, J. C., T. Herbert, M. Kashgarian, and C. Charles (2010), Intermediate and deep water mass distribution in the Pacific during the Last Glacial Maximum inferred from oxygen and carbon stable isotopes, *Quat. Sci. Rev.*, *29*(9–10), 1228–1245.
Horikawa, K., Y. Asahara, K. Yamamoto, and Y. Okazaki (2010), Intermediate water formation in the Bering Sea during glacial periods: Evidence from neodymium isotope ratios, *Geology*, *38*(5), 435–438.
Jian, Z., and L. Wang (1997), Late quaternary benthic foraminifera and deep-water paleoceanography in the South China Sea, *Mar. Micropaleontol.*, *32*(1–2), 127–154.
Jian, Z., L. Wang, M. Kienast, M. Sarnthein, W. Kuhnt, H. Lin, and P. Wang (1999), Benthic foraminiferal paleoceanography of the South China Sea over the last 40,000 years, *Mar. Geol.*, *156*(1–4), 159–186.
Kawabe, M., and S. Fujio (2010), Pacific ocean circulation based on observation, *J. Oceanogr.*, *66*(3), 389–403.
Keigwin, L. D. (1998), Glacial-Age Hydrography of the Far Northwest Pacific Ocean, *Paleoceanography*, *13*(4), 323–339, doi:10.1029/98PA00874.
Keigwin, L. D. (2004), Radiocarbon and stable isotope constraints on Last Glacial Maximum and Younger Dryas ventilation in the western North Atlantic, *Paleoceanography*, *19*, PA4012, doi:10.1029/2004PA001029.
Keir, R. S., and R. L. Michel (1993), Interface dissolution control of the ^{14}C profile in marine sediment, *Geochim. Cosmochim. Acta*, *57*(15), 3563–3573.
Key, R. M., A. Kozyr, C. L. Sabine, K. Lee, R. Wanninkhof, J. L. Bullister, R. A. Feely, F. J. Millero, C. Mordy, and T. H. Peng (2004), A global ocean carbon climatology: Results from Global Data Analysis Project (GLODAP), *Global Biogeochem. Cycles*, *18*, GB4031, doi:10.1029/2004GB002247.
Köhler, P., H. Fischer, G. Munhoven, and R. E. Zeebe (2005), Quantitative interpretation of atmospheric carbon records over the last glacial termination, *Global Biogeochem. Cycles*, *19*, GB4020, doi:10.1029/2004GB002345.
Laj, C., P. Wang, and Y. Balut (2005), IPEV les rapports de campagnes à la mer, MD147/MARCO POLO–IMAGES XII à bord du "Marion Dufresne," 59 pp.
Lisiecki, L. E., and M. E. Raymo (2005), A Pliocene-Pleistocene stack of 57 globally distributed benthic $\delta^{18}O$ records, *Paleoceanography*, *20*, PA1003, doi:10.1029/2004PA001071.
Lüdmann, T., H. K. Wong, and K. Berglar (2005), Upward flow of North Pacific Deep Water in the northern South China Sea as deduced from the occurrence of drift sediments, *Geophys. Res. Lett.*, *32*, L05614, doi:10.1029/2004GL021967.
Lund, D. C., A. C. Mix, and J. Southon (2011), Increased ventilation age of the deep northeast Pacific Ocean during the last deglaciation, *Nat. Geosci.*, *4*(11), 771–774.
Marchitto, T. M., S. J. Lehman, J. D. Ortiz, J. Flückiger, and A. van Geen (2007), Marine radiocarbon evidence for the mechanism of deglacial atmospheric CO_2 rise, *Science*, *316*(5830), 1456–1459.
Matsumoto, K., and J. Lynch-Stieglitz (1999), Similar glacial and holocene deep water circulation inferred from Southeast Pacific Benthic foraminiferal carbon isotope composition, *Paleoceanography*, *14*(2), 149–163, doi:10.1029/1998PA900028.
Matsumoto, K., T. Oba, J. Lynch-Stieglitz, and H. Yamamoto (2002), Interior hydrography and circulation of the glacial Pacific Ocean, *Quat. Sci. Rev.*, *21*(14–15), 1693–1704.
Max, L., L. Lembke-Jene, J.-R. Riethdorf, R. Tiedemann, D. Nürnberg, H. Kühn, and A. Mackensen (2013), Pulses of enhanced North Pacific Intermediate Water ventilation from the Okhotsk Sea and Bering Sea during the last deglaciation, *Clim. Dyn.*, *9*(6), 6221–6253.
McManus, J. F., R. Francois, J. M. Gherardi, L. D. Keigwin, and S. Brown-Leger (2004), Collapse and rapid resumption of Atlantic meridional circulation linked to deglacial climate changes, *Nature*, *428*(6985), 834–837.
Mekik, F. (2014), Radiocarbon dating of planktonic foraminifer shells: A cautionary tale, *Paleoceanography*, *29*, 13–29, doi:10.1002/2013PA002532.
Menviel, L., A. Timmermann, O. Elison Timm, A. Mouchet, A. Abe-Ouchi, M. O. Chikamoto, N. Harada, R. Ohgaito, and Y. Okazaki (2012), Removing the North Pacific halocline: Effects on global climate, ocean circulation and the carbon cycle, *Deep Sea Res., Part II*, *61–64*(0), 106–113.
Miao, Q., R. C. Thunell, and D. M. Anderson (1994), Glacial-Holocene carbonate dissolution and sea surface temperatures in the south China and Sulu Seas, *Paleoceanography*, *9*(2), 269–290, doi:10.1029/93PA02830.
Minoshima, K., H. Kawahata, T. Irino, K. Ikehara, K. Aoki, M. Uchida, M. Yoneda, and Y. Shibata (2007), Deep water ventilation in the northwestern North Pacific during the last deglaciation and the early Holocene (15–5 cal kyr B.P.) based on AMS ^{14}C dating, *Nucl. Instrum. Methods Phys. Res., Sect. B*, *259*(1), 448–452.
Monnin, E., A. Indermühle, A. Dällenbach, J. Flückiger, B. Stauffer, T. F. Stocker, D. Raynaud, and J.-M. Barnola (2001), Atmospheric CO_2 concentrations over the last glacial termination, *Science*, *291*(5501), 112–114.
Negre, C., R. Zahn, A. L. Thomas, P. Masque, G. M. Henderson, G. Martinez-Mendez, I. R. Hall, and J. L. Mas (2010), Reversed flow of Atlantic deep water during the Last Glacial Maximum, *Nature*, *468*(7320), 84–88.
Ohkushi, K. I., T. Itaki, and N. Nemoto (2003), Last Glacial–Holocene change in intermediate-water ventilation in the Northwestern Pacific, *Quat. Sci. Rev.*, *22*(14), 1477–1484.
Okazaki, Y., A. Timmermann, L. Menviel, N. Harada, A. Abe-Ouchi, M. O. Chikamoto, A. Mouchet, and H. Asahi (2010), Deepwater Formation in the North Pacific During the Last Glacial Termination, *Science*, *329*(5988), 200–204.
Okazaki, Y., T. Sagawa, H. Asahi, K. Horikawa, and J. Onodera (2012), Ventilation changes in the western North Pacific since the last glacial period, *Clim. Past*, *8*(1), 17–24.
Oppo, D. W., and R. G. Fairbanks (1987), Variability in the deep and intermediate water circulation of the Atlantic Ocean during the past 25,000 years: Northern Hemisphere modulation of the Southern Ocean, *Earth Planet. Sci. Lett.*, *86*(1), 1–15.
Qu, T., J. B. Girton, and J. A. Whitehead (2006), Deepwater overflow through Luzon Strait, *J. Geophys. Res.*, *111*, C01002, doi:10.1029/2005jc003139.
Rae, J. W. B., M. Sarnthein, G. L. Foster, A. Ridgwell, P. M. Grootes, and T. Elliott (2014), Deep water formation in the North Pacific and deglacial CO_2 rise, *Paleoceanography*, *29*, 645–667, doi:10.1002/2013PA002570.
Reimer, P. J., et al. (2013), IntCal13 and Marine13 Radiocarbon Age Calibration Curves 0–50,000 Years cal BP, *Radiocarbon*, *55*(4), 1869–1887.
Rella, S. F., R. Tada, K. Nagashima, M. Ikehara, T. Itaki, K. I. Ohkushi, T. Sakamoto, N. Harada, and M. Uchida (2012), Abrupt changes of intermediate water properties on the northeastern slope of the Bering Sea during the last glacial and deglacial period, *Paleoceanography*, *27*, PA3203, doi:10.1029/2011PA002205.

Sagawa, T., and K. Ikehara (2008), Intermediate water ventilation change in the subarctic northwest Pacific during the last deglaciation, *Geophys. Res. Lett.*, *35*, L24702, doi:10.1029/2008GL035133.
Sarnthein, M. (2011), Northern Meltwater Pulses, CO_2, and Changes in Atlantic Convection, *Science*, *331*(6014), 156–158.
Sarnthein, M., P. M. Grootes, J. P. Kennett, and M.-J. Nadeau (2007), ^{14}C reservoir ages show deglacial changes in ocean currents and carbon cycle, *AGU Geophys. Monogr.*, *173*, 175–196.
Sarnthein, M., B. Schneider, and P. M. Grootes (2013a), Peak glacial ^{14}C ventilation ages suggest major draw-down of carbon into the abyssal ocean, *Clim. Past*, *9*, 2595–2614.
Sarnthein, M., H. Sadatzki, and Z. Jian (2013b), Stratigraphic gaps at northern South China Sea margin reflect changes in Pacific deepwater inflow at glacial Termination II, *Sci. China Earth Sci.*, *56*(10), 1748–1758.
Schmitz, W. J. (1996), On the world ocean circulation, Volume II, *the Pacific and Indian Oceans/a global update Rep*., Woods Hole Oceanographic Institution.
Sigman, D. M., and E. A. Boyle (2000), Glacial/interglacial variations in atmospheric carbon dioxide, *Nature*, *407*(6806), 859–869.
Skinner, L. C., S. Fallon, C. Waelbroeck, E. Michel, and S. Barker (2010), Ventilation of the deep Southern Ocean and deglacial CO_2 rise, *Science*, *328*(5982), 1147–1151.
Southon, J., M. Kashgarian, M. Fontugne, B. Metivier, and W. W.-S. Yim (2002), Marine reservoir corrections for the Indian Ocean and Southeast Asia, *Radiocarbon*, *44*(1), 167–180.
Steinke, S., C. Glatz, M. Mohtadi, J. Groeneveld, Q. Li, and Z. Jian (2011), Past dynamics of the East Asian monsoon: No inverse behaviour between the summer and winter monsoon during the Holocene, *Global Planet. Change*, *78*(3–4), 170–177.
Stott, L., J. Southon, A. Timmermann, and A. Koutavas (2009), Radiocarbon age anomaly at intermediate water depth in the Pacific Ocean during the last deglaciation, *Paleoceanography*, *24*, PA2223, doi:10.1029/2008PA001690.
Su, J. (2004), Overview of the South China Sea circulation and its influence on the coastal physical oceanography outside the Pearl River Estuary, *Cont. Shelf Res.*, *24*(16), 1745–1760.
Tachikawa, K., and H. Elderfield (2002), Microhabitat effects on Cd/Ca and $\delta^{13}C$ of benthic foraminifera, *Earth Planet. Sci. Lett.*, *202*(3–4), 607–624.
Thornalley, D. J. R., S. Barker, W. S. Broecker, H. Elderfield, and I. N. McCave (2011), The deglacial evolution of North Atlantic deep convection, *Science*, *331*(6014), 202–205.
Thunell, R. C., M. Qingmin, S. E. Calvert, and T. F. Pedersen (1992), Glacial-Holocene biogenic sedimentation patterns in the South China Sea: Productivity variations and surface water pCO_2, *Paleoceanography*, *7*(2), 143–162, doi:10.1029/92PA00278.
Tian, J., Q. Yang, X. Liang, L. Xie, D. Hu, F. Wang, and T. Qu (2006), Observation of Luzon Strait transport, *Geophys. Res. Lett.*, *33*, L19607, doi:10.1029/2006GL026272.
Tian, J., Q. Yang, and W. Zhao (2009), Enhanced diapycnal mixing in the South China Sea, *J. Phys. Oceanogr.*, *39*(12), 3191–3203.
Tian, J., E. Huang, and D. K. Pak (2010), East Asian winter monsoon variability over the last glacial cycle: Insights from a latitudinal sea-surface temperature gradient across the South China Sea, *Palaeogeogr. Palaeoclimatol. Palaeoecol.*, *292*(1–2), 319–324.
Wang, L., M. Sarnthein, H. Erlenkeuser, J. Grimalt, P. Grootes, S. Heilig, E. Ivanova, M. Kienast, C. Pelejero, and U. Pflaumann (1999), East Asian monsoon climate during the Late Pleistocene: High-resolution sediment records from the South China Sea, *Mar. Geol.*, *156*(1–4), 245–284.
Wang, Y. J., H. Cheng, R. L. Edwards, Z. S. An, J. Y. Wu, C.-C. Shen, and J. A. Dorale (2001), A high-resolution absolute-dated late Pleistocene monsoon record from Hulu Cave, China, *Science*, *294*(5550), 2345–2348.
Wang, Y., H. Cheng, R. L. Edwards, Y. He, X. Kong, Z. An, J. Wu, M. J. Kelly, C. A. Dykoski, and X. Li (2005), The Holocene Asian monsoon: Links to solar changes and North Atlantic climate, *Science*, *308*(5723), 854–857.
Wei, G., C.-Y. Huang, C.-C. Wang, M.-Y. Lee, and K.-Y. Wei (2006), High-resolution benthic foraminifer $\delta^{13}C$ records in the South China Sea during the last 150 ka, *Mar. Geol.*, *232*(3–4), 227–235.
Wyrtki, K. (1961), Physical oceanography of the Southeast Asian waters, *NAGA Rep. 2*, pp. 1–195, La Jolla, Calif.
Yasuda, I. (1997), The origin of the North Pacific Intermediate Water, *J. Geophys. Res.*, *102*(C1), 893–909, doi:10.1029/96JC02938.
Yu, J., W. S. Broecker, H. Elderfield, Z. Jin, J. McManus, and F. Zhang (2010a), Loss of carbon from the deep sea since the last glacial maximum, *Science*, *330*(6007), 1084–1087.
Yu, J., R. F. Anderson, Z. Jin, J. W. B. Rae, B. N. Opdyke, and S. M. Eggins (2013), Responses of the deep ocean carbonate system to carbon reorganization during the last glacial–interglacial cycle, *Quat. Sci. Rev.*, *76*(0), 39–52.
Yu, K., J. Zhao, P. Wang, Q. Shi, Q. Meng, K. D. Collerson, and T. Liu (2006), High-precision TIMS U-series and AMS ^{14}C dating of a coral reef lagoon sediment core from southern South China Sea, *Quat. Sci. Rev.*, *25*(17–18), 2420–2430.
Yu, K., Q. Hua, J.-X. Zhao, E. Hodge, D. Fink, and M. Barbetti (2010b), Holocene marine ^{14}C reservoir age variability: Evidence from ^{230}Th-dated corals in the South China Sea, *Paleoceanography*, *25*, PA3205, doi:10.1029/2009PA001831.
Zhao, W., C. Zhou, J. Tian, Q. Yang, B. Wang, L. Xie, and T. Qu (2014), Deep water circulation in the Luzon Strait, *J. Geophys. Res. Oceans*, *119*, 790–804, doi:10.1002/2013jc009587.